Nanoscale

PAPER

View Article Online
View Journal | View Issue

Cite this: *Nanoscale*, 2025, **17**, 19210

Computational evaluation of structural and chemical possibilities exposed by Ti_2CT_x nanoribbons and 2D-nanoparticles†

Yamilée Morency and Aleksandra Vojvodic *

MXenes are a rapidly expanding family of 2D materials known for their unique tunability, yet studies of their edges remain sparse compared to their better-characterized basal planes. Herein, we use density functional theory (DFT) to computationally investigate the structural and chemical properties of Ti_2CT_x nanoribbons and 2D-nanoparticles. Our findings reveal that under-coordinated edge atoms exhibit stability and reactivity distinct from that forming the basal planes, driven by edge symmetry and environmental chemical potentials. Specifically, the constructed stability diagrams and Wulff constructions illustrate how 2D-nanoparticle morphologies and edge terminations evolve under different hydrogen chemical potentials. Reducing conditions favor fluorine terminations, while oxidizing environments stabilize oxygen-terminated edges. Hydrogen adsorption analysis highlights unique edge-specific chemistries, with certain terminations achieving hydrogen evolution reaction (HER) overpotentials comparable to those of the previously identified basal planes of Mo_2C MXene. Notably, our study identifies the {010} and {110} edges as highly active catalytic sites under specific conditions, emphasizing the role of edge under-coordination in dictating catalytic behavior. These results underscore the potential of MXene edges for tailoring properties beyond the basal plane, providing pathways for designing next-generation materials for catalysis, energy, and environmental applications.

Received 3rd January 2025,
Accepted 3rd July 2025

DOI: 10.1039/d5nr00026b

rsc.li/nanoscale

1 Introduction

In the last decade, we have seen the rise of MXenes[1–3] which now form a large group of highly tunable 2D materials with unique properties in numerous applications. The formula of a stoichiometric MXene is $M_{n+1}X_nT_x$, where M is a transition metal, X is carbon or nitrogen, T_x is the termination group,[4] and n is an integer. The properties of MXenes can be tuned by modifying the crystal structure by changing n, both of the chemical constituents, *i.e.*, the transition metal and the X atom, and importantly the terminating group. In this paper, we systematically study an additional degree of tunability in MXenes, namely the under-coordinated atoms present on the edges, and the role of this reduced dimensionality in the material. As of now, only a few studies have focused on MXene edges.[5–7] Instead, most studies of MXenes have focused on the properties and chemistry of the basal planes of these 2D materials. This initial approach is reasonable because MXenes have a high surface-to-volume ratio and would allow for easier technological scale-up. However, in reality, MXenes are not infinite 2D sheets but appear as flakes or nanoparticles of varying sizes with exposed edges.[8] The properties and chemistry of the edges in other 2D materials have been shown to potentially differ from those of basal planes. A notable example of this is the 2D dichalcogenide MoS_2 [9–12] where the stoichiometric basal planes are chemically and catalytically inert while the 1D edges are catalytically active sites for the hydrogen evolution reaction (HER)[13,14] and hydrodesulfurization (HDS).[15,16] In recent years, edges have also been investigated in a number of 2D materials including graphene[17,18] and hexagonal boron nitride[19] to name a few. This raises the question of how MXene edges might contribute to the overall properties and performance of the material and how those would compare to other known 2D materials.

In this paper, we investigate and establish the fundamental similarities and differences of under-coordinated atoms exposed at the edges and contrast them to the atoms of the basal plane of an MXene. Specifically, we focus on understanding the stability and chemistry of different possible edges. We used functionalized Ti_2C as a prototype MXene material because it is the MXene that most closely resembles MoS_2 and graphene, which are common materials in edge studies. We used density functional theory (DFT) simulations to model two

Department of Chemical and Biomolecular Engineering, University of Pennsylvania, Philadelphia, PA 19104, USA. E-mail: alevoj@seas.upenn.edu

† Electronic supplementary information (ESI) available. See DOI: https://doi.org/10.1039/d5nr00026b

types of MXene systems with edges: nanoribbons and 2D-nanoparticles. From the obtained *ab initio* energetics, we identified the most thermodynamically favorable edges under different environmental conditions. We then studied the chemical properties of these stable edges using hydrogen adsorption as a probe for reactivity and the hydrogen evolution reaction as a probe for activity. The focus on hydrogen chemistry is because the basal planes of MXenes have been found to have HER capabilities – see the discovery of Mo_2C by a team including one of the authors[20] – and hydrogen adsorption is an integral step in numerous electrochemical and thermal catalytic processes.

We demonstrate that the structural and chemical properties of the MXene edges are vastly different from those of the basal planes. Importantly, we also show that the edge properties are different and depend on the symmetry of the edges, *i.e.* different Miller indices and terminations, and we identify the unique edge-dependent chemistry. These findings illustrate that under-coordination plays a crucial role in the chemistry of an MXene and could allow the design of MXene materials with properties different from those of their basal planes. From a material discovery standpoint, our results suggest that the role of under-coordination present in MXene 2D-nanoparticles could open up completely new chemistry avenues not present in other 2D materials as MXenes have the benefit of a large structural and morphological diversity.

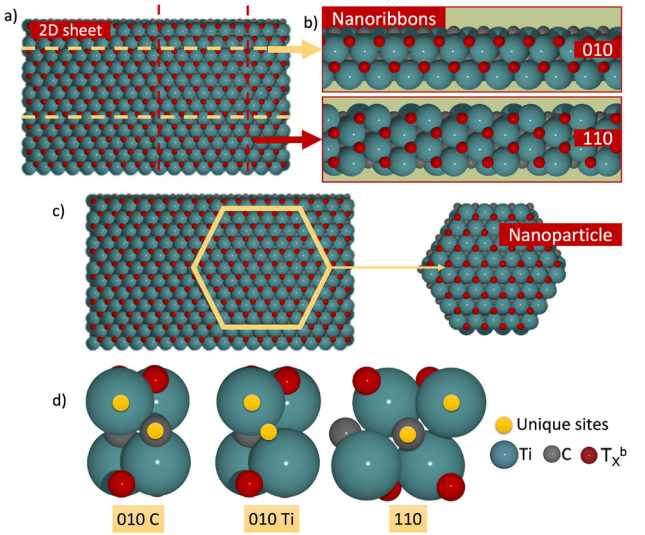

Fig. 1 Different MXene structural models (top down view) of (a) a 2D sheet with dashed lines indicating different cuts and (b) two different nanoribbons with their exposed edges. The top inset shows the {010} nanoribbon with exposed Ti and C edges and the bottom inset shows the {110} NP with an exposed mixed Ti–C edge termination. (c) An example of an explicit hexagonal MXene nanoparticle cut from the 2D sheet. (d) Potential adsorption sites on different MXene edges (side view) as exemplified with O as the functional group on the basal plane.

2 Theoretical and computational frameworks

2.1 Physical models of MXenes

A 2D MXene sheet (see Fig. 1(a)) can be cut, exposing different edges, which can be described using Miller indices. Each index corresponds to an angle α[17] given by:

$$\alpha = \cos^{-1}\left(\sqrt{\frac{3(m+n)^2}{4((m+n)^2 - mn)}}\right), \quad (1)$$

where α is the angle formed with an arbitrary 0 and m and n are the first two Miller indices that describe the edge; the third Miller index is kept at 0 because Ti_2C is 2D. This paper focuses on the lower Miller index edges: the {010} and {110} cuts of Ti_2CT_x, commonly known as the armchair and the zigzag edges.[21–23] We chose to study the lower Miller index because these edges provide a simpler structural foundation for analysis, allowing us to establish fundamental insights and develop baseline models before exploring higher-index edges, which often involve more complex atomic arrangements or reconstruction.

We studied MXene edges using two models: nanoribbons (also known as stripes) and 2D-nanoparticles. Nanoribbons (NRs) are composed of a basal plane and two edges. They are infinite in one direction and finite in the other two directions. 2D-nanoparticles (NPs) are also composed of a basal plane and edges but are finite in every direction. As illustrated in Fig. 1(b), the stoichiometric {010} nanoribbons have two types of edge terminations: Ti and C. To create symmetric NRs, we adjusted these stripes by adding or removing a C atom to form either a C-terminated or a Ti-terminated ribbon, thereby ensuring symmetry and decoupling of the two edge types for independent analysis. In contrast, the {110} NRs feature two identical edges upon the formation of a cut, terminated by one C atom and two Ti atoms.

MXenes are terminated at the basal plane with a functional group T_x^b, resulting in a chemical formula Ti_2CT_x.[4,24] This gives an additional degree of freedom when designing the material and allows for potentially different chemistry to be tapped into. However, it also introduces an additional level of computational complexity to be probed. The functional group T_x^b is highly synthesis dependent and can be a simple termination group like –O, –Cl, –F, and –OH,[4] or a more complicated one like an alkyl chain.[25] We focus on the most common termination groups: –O, –OH, and –F. Given that synthesized MXenes typically possess functional groups on their basal planes, it is reasonable to hypothesize that the edges of MXenes, with their exposed under-coordinated sites, might also undergo termination to satisfy unsaturated bonds. Consequently, we consider two edge models: (i) bare edges, where edge atoms remain unsaturated as they would in an idealized cut from an infinite 2D material; and (ii) functionalized edges, where edge atoms are terminated with different functional groups, including –O, –OH, –F, and –H. They incrementally adsorb different quantities of a functional group on the edges until all sites are fully occupied or the adsorption

energy (E_{ads}) of the terminating group exceeds 0, indicating that further adsorption is unfavorable. The optimal coverage of these functional groups is expected to depend on environmental conditions and is thus determined through the construction of a stability diagram. Fig. 1(d) shows the high-symmetry adsorption sites considered in this study.

It is computationally intractable to cover the entirety of the 2D-nanoparticle shape space coupled with all the possible termination and edge combinations. For a first approximation, MXene 2D-nanoparticles are composed of edges and a basal plane. We can make predictions about the functionality of thermodynamically stable MXene 2D-nanoparticles using edge formation energy γ (see the calculation details below) of the nanoribbons and Wulff constructions.[26] Wulff constructions determine the equilibrium shape of a 2D nanoparticle from the edge formation energy and the angle α associated with the Miller index. To build a Wulff construction, the points (γ, α) are plotted in a polar coordinate system. A line perpendicular to (0, 0) (γ, α) through the point (γ, α) is drawn. This is repeated for all points. The smallest shape through which no line passes indicates the equilibrium of the nanoparticles. We follow the framework described in ref. 9 and 17 to build the Wulff constructions of the MXenes in this paper.

2.2 *Ab initio* thermodynamics

We assume, to a first approximation, that edge functionalization occurs through:

$$(Ti_2CT_x)_y + 2H_2O \rightarrow (Ti_2CT_x)_yO_2 + 2H_2 \quad (2)$$

$$(Ti_2CT_x)_y + 2H_2O \rightarrow (Ti_2CT_x)_y(OH)_2 + H_2 \quad (3)$$

$$(Ti_2CT_x)_y + 2HF \rightarrow (Ti_2CT_x)_yF_2 + H_2 \quad (4)$$

$$(Ti_2CT_x)_y + H_2 \rightarrow (Ti_2CT_x)_yH_2 \quad (5)$$

where $T_x{}^b$ = {bare, O, OH, and F} and y corresponds to the number of formula units of MXenes in the stripe. These reactions allow the chemical potentials of the possible terminating groups (–O, –F, and –OH) to all be related to the chemical potential of H, μ_H and the solvated formation energies for the liquid from the gaseous molecules through the following equations:[24]

$$\mu_O = \Delta G_{f_{H_2O}} - 2\mu_H, \quad (6)$$

$$\mu_{OH} = \Delta G_{f_{H_2O}} - \mu_H, \quad (7)$$

$$\mu_F = \Delta G_{f_{HF}} - \mu_H. \quad (8)$$

We are using HF, H_2O and H_2 as the references to calculate the adsorption energies of the adsorbates which become the functional groups on both the edges and the basal planes. The values for $\Delta G_{f_{H_2O}}$ and $\Delta G_{f_{HF}}$ are taken to be the experimental formation energies, namely

$$\Delta G_{f_{HF}} = -2.81 \text{ eV}, \quad (9)$$

$$\Delta G_{f_{H_2O}} = -2.51 \text{ eV}. \quad (10)$$

The lower limit of μ_H is taken to be the range of the possible values of the chemical potentials which here is −1.255 eV and the upper limit is set to 0 eV. (The value of the chemical potential of H_2 gas.)

The propensity for the edges to adsorb terminating groups will depend on the adsorption energy given by:

$$E_{T_{ads}} = E_{MXene+H} - E_{MXene} - \frac{1}{2}E_{H_2}. \quad (11)$$

By plotting the edge formation energy, γ, as a function of the chemical potential, we create a stability diagram that identifies the most thermodynamically favorable structural configuration at different μ_H values. This approach allows us to predict the stability of different edge terminations with respect to the concentration of oxygen. The edge formation energy for the NR model is given by:

$$\gamma = \frac{1}{2L}\left(E_{stripe} - \frac{N_M}{2}E_{bulk} - N_{e_{T_xb}}\mu_{e_{T_xb}}\right), \quad (12)$$

where L is the length of the edge, E_{stripe} is the energy of the stripe, E_{bulk} is the energy of the infinite 2D sheet without cuts, $N_{e_{T_x}}$ is the number of species covering the edge and $\mu_{e_{T_x}}$ is the chemical potential of the abovementioned species. The general formula for this equation is given by:

$$\gamma = \frac{1}{2L}(E_{stripe} - N_{bulk}E_{bulk} - N_{T_x}E_{T_x} - N_ME_M - N_XE_X - N_{e_{T_x}}\mu_{e_{T_x}}). \quad (13)$$

The oxygen chemical potential is related to the oxygen partial pressure through the equation:

$$\mu_{O_2} = \mu_{O_2}{}^0 + k_bT\ln\left(\frac{p_{O_2}}{p^0}\right). \quad (14)$$

Fig. 1(d) shows a potential shape an MXene nanoparticle could take on, namely a hexagon. However, there are a number of configurations that a 2D nanoparticle can potentially take including a triangular shape, a dodecagon, *etc*. We used Wulff constructions to determine the most thermodynamically favorable shape for the Ti_2CT_x NPs we study in this paper. Using the stability diagrams in tandem with a Wulff construction, we can also determine the equilibrium shape of the NPs as a function of their environment as measured through the chemical potential.

The chemical properties of the stable edges are probed using hydrogen adsorption. Specifically, we calculate hydrogen adsorption for the basal planes of Ti_2CT_x 2D sheets, nanoribbons, and nanoparticles at the adsorption sites, as shown in Fig. 1(d). We also calculate hydrogen adsorption at the edges. Hydrogen adsorption energy is given by:

$$E_{H_{ads}} = E_{MXene+H} - E_{MXene} - \frac{1}{2}E_{H_2}. \quad (15)$$

An adsorption energy value of less than 0 eV indicates that hydrogen adsorption is favorable, whereas a H adsorption

energy value larger than 0 eV means that hydrogen adsorption is unfavorable. This insight into hydrogen adsorption can be extended to determine the overpotential for the hydrogen evolution reaction of these structures using a computational hydrogen electrode.[27,28]

2.3 Computational methods

All calculations in this paper were performed using the DFT code Quantum Espresso[29,30] and the BEEF–vdW exchange–correlation functional.[31] We used a 1 × 11 supercell with physical structures, as shown in Fig. 1. To avoid interactions between the repeating layers, a vacuum of 20 Å was applied to both the z and y directions. A Monkhorst–Pack k-point mesh of 4 × 1 × 1 was used. The convergence criterion was set to 1×10^{-6} eV. The energy cut-off for all calculations is 700 eV. We have ensured that the nanoribbon basal planes are converged with respect to the nanoribbon width, effectively decoupling the two edges, as shown in Fig. S1 in the ESI.†

3 Results

The goal of this paper is to determine the shape and termination (basal planes and edges) of MXene nanoribbons and nanoparticles. To achieve this, we first analyze how edge termination (T_x^e) varies with respect to basal plane termination (T_x^b), using the adsorption energy normalized per adsorbate of the edge termination as the metric ($E_{T_x^e}$). Subsequently, we use the chemical potential of hydrogen (μ_H) to investigate how basal plane terminations change with the oxygen partial pressure, using a stability diagram. We then calculate the adsorption free energy of edges for terminations that are favorable under reducing (high μ_H) and oxidizing (low μ_H) conditions. Briefly, our results show that under reducing conditions (below $\mu_H = -1.02$ eV), the basal plane is F-terminated, while under oxidizing conditions (above $\mu_H = -1.02$ eV), the basal plane becomes O-terminated. We construct stability diagrams for F- and O-terminations to determine the $\{T_x^e, T_x^b\}$ pairs exposed at different chemical potentials. We then combine these stability diagrams with the stability diagram of the basal plane terminations to get a more complete picture of the edge and basal plane terminations of the nanoribbons. Finally, we use Wulff constructions to determine the shape, edge termination, and coverage of the Ti_2CT_x nanoparticles and the oxygen partial pressures highlighted in the stability diagrams.

3.1 Adsorption energy of functional groups on edges with varying basal plane terminations

Fig. 2 shows how the adsorption energies of functional groups on the edges of the {010} C, {010} Ti and {110} MXene NRs change with respect to different functional groups on the basal planes. Specifically, the basal plane terminations are taken to be T_x^b = bare, OH, O, and F (Fig. 2a–d, respectively) for the edge terminating groups T_x^e = O, OH, and F. The edge termination T_x^e is adsorbed onto the edge with a coverage of up to 2 atoms/edge or until the T_x^e adsorption energy is larger than 0 eV. The coverage is limited to 2 atoms/edge because that is the maximum coverage at which all the edges do not present any large reconstruction (Fig. S2 in the ESI† – for example, if a {110} edge has 2 atoms/edge, one of the O atoms will penetrate the edge replacing the C atom while another O atom attacks the C atom to form a carbon moiety similar to the one seen for the C edge); this allows for an apples-to-apples comparison of all the edges.

The most important finding is that the edges, just as the basal planes, will always be terminated with some quantity of edge functional groups T_x^e; however, the exact coverage depends on what the functional group of the specific element (s) consists of and the nature of the reactivity of the considered edge. Fig. 2 shows the thermodynamics of different T_x^e coverages for each considered edge and its dependence on the functional group of the basal plane T_x^b.

For the {010} C edge, the edge termination is heavily influenced by the basal plane termination. When the basal plane is bare, the edge is terminated by 1 ML of F. When the basal plane is terminated by hydroxyl groups (T_x^b = OH), the C edge is terminated by 1 or 2 MLs of O, with overlapping adsorption energies. This overlap indicates that the addition of a second oxygen atom to the C edge does not significantly affect the average adsorption energy. In contrast, when the basal plane is terminated by oxygen (T_x^b = O) or fluorine (T_x^b = F), the C edge is consistently terminated by 1 ML of O. Importantly, this edge oxygen forms a carbonyl (CO) moiety with the exposed carbon atom at the edge. The bond lengths of the CO moiety vary depending on the basal plane termination, measuring 1.163 Å for T_x^b = O, 1.237 Å for T_x^b = OH, and 1.325 Å for T_x^b = F. In the case of T_x^b = F, visually, one might argue that no CO moiety is present, rather, the adsorption of O onto an edge Ti atom occurs. T_x^b completely changed the bonding of O to the {010} C edge. Given that the equilibrium bond length of the CO bond is 1.128 Å,[32] we see that there is elongation of the bond, which indicates that the CO moiety is adsorbed to the edge or is essentially part of the edge. From this, we see that edge chemistry is significantly affected by the basal plane termination (T_x^b).

For the {010} Ti edge, the basal plane termination similarly dictates the edge termination chemistry. When the basal plane is bare, the edge is terminated by 2 MLs of O. In the presence of T_x^b = OH, the edge can be terminated by 1 or 2 MLs of F, as both configurations exhibit equivalent adsorption energies. When the basal plane is terminated by oxygen (T_x^b = O), the edge is terminated by 1 ML of F. Interestingly, when the basal plane is terminated by fluorine (T_x^b = F), the {010} Ti edge behaves similarly to when T_x^b = OH, with the termination 1 or 2 MLs of F being favorable.

For the {110} edge, the edge termination trend is also dependent on the basal plane termination. When the basal plane is bare, the {110} edge is terminated by 2 MLs of O. In contrast, with hydroxyl termination (T_x^b = OH), the edge is terminated by 1 ML of H. When the basal plane is terminated by oxygen (T_x^b = O), the edge is terminated by 2 MLs of F. Finally,

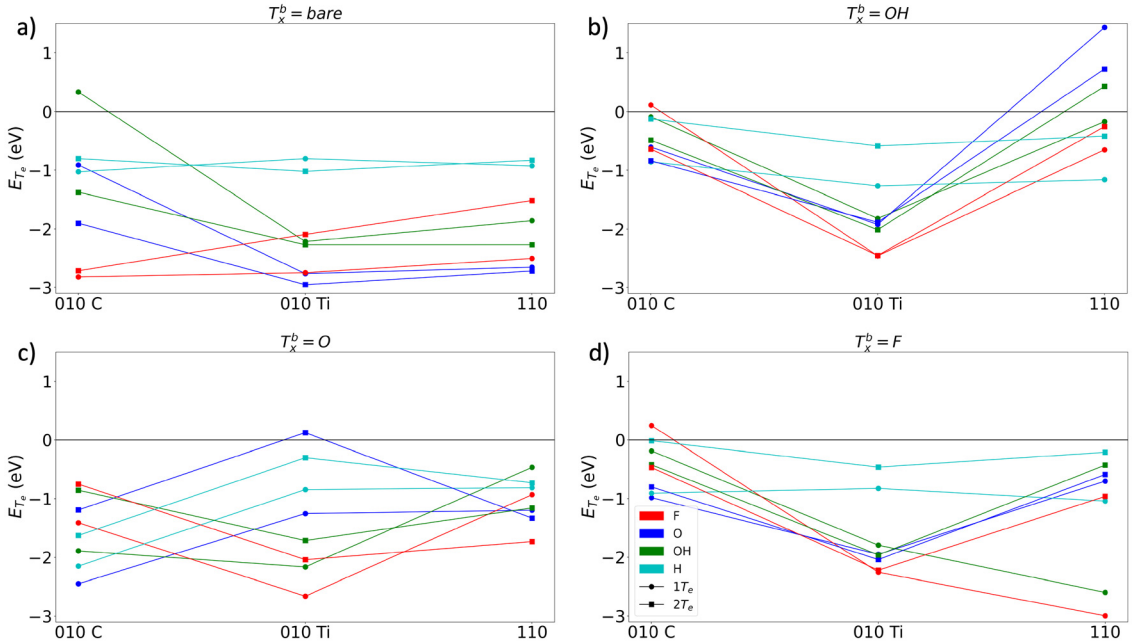

Fig. 2 Calculated adsorption energy normalized per adsorbate $E_{T_x^e}$ of the edge terminations (O, F, and OH) of the {010} C, {010} Ti and {110} MXene NRs as a function of different basal plane terminations (T_x^b) being (a) bare basal plane, (b) T_x^b = OH, (c) T_x^b = O, and (d) T_x^b = F.

when the basal plane is terminated by fluorine (T_x^b = F), the edge is terminated by 1 ML of F.

While these predictions provide insight into edge termination trends based solely on adsorption energy, it is important to note that these configurations may not fully reflect real-world behavior, as they do not account for environmental conditions. To address this, the following section considers how specific experimental conditions, particularly the chemical potential of hydrogen, influence the stability and termination of the edges as present in nanoribbons.

3.2 Adsorption free energy of terminations on MXenes

3.2.1 Functionalizing basal planes. Since a nanoribbon is composed of a basal plane and edges, we must first determine how (if at all) the basal plane present in a nanoribbon has the same termination as or different terminations to the basal plane of an infinite 2D MXene sheet or not (which is done in this section), and then compare if the basal plane of the nanoribbon has the same termination as or different termination to the edges (in the following sections).

Fig. 3 shows the calculated binding energies of various T_x^b terminations as a function of the hydrogen chemical potential μ_H. These values were computed using the approach described in ref. 24. In all three nanoribbons, the most favorable termination at high μ_H values (more reducing environments) is fluorine, while under more oxidizing conditions (lower μ_H), the oxygen termination becomes favored. Notably, however, the critical μ_H value at which the preferred termination shifts from F to O differs depending on the edge orientation of the nanoribbon; this transition occurs at μ_H = −1.0 eV for the {010} C nanoribbon, μ_H = −1.1 eV for the {110} MXene, and μ_H = −1.2 eV for the {010} Ti nanoribbon. This variation in transition points highlights a key finding: the nature of the edge modifies the relative stability of terminations on the basal plane. In other words, the interaction between the edge and the basal plane is not negligible – edges influence the thermodynamics of basal termination and *vice versa*. This is likely due to long-range electronic or structural effects imposed by the edges on the nearby basal atoms. Given the thermodynamic relationships between μ_H, μ_O, and the partial pressure of oxygen (p_{O_2}) *via* eqn (6)–(8), these results also suggest that the oxygen partial pressure required to stabilize O-terminated basal planes is edge dependent. Thus, synthesis or treatment conditions could result in different basal terminations for nanoribbons of different edge orientations, even under the

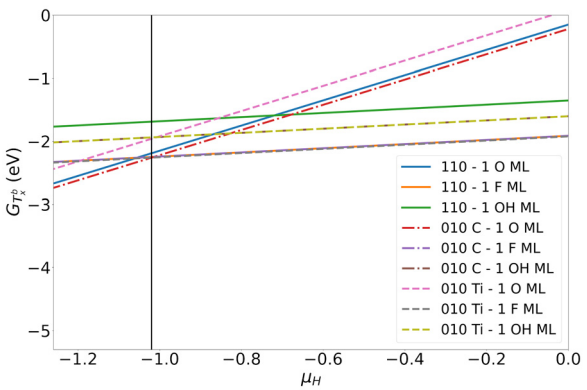

Fig. 3 Stability of different basal plane terminations for the {010} C, {010} Ti, and {110} NRs of $Ti_2CT_x^b$ with T_x^b = O, OH, and F.

same environmental conditions. In all the studied nanoribbons, OH terminations are not thermodynamically favored across the full range of μ_H considered. While mixed terminations are not explicitly considered here, isolating single-termination cases allows us to identify trends in chemical behavior and highlight edge–basal coupling effects.

3.2.2 Functionalizing edges. Fig. 4 illustrates how the exposed edge and its subsequent functional group coverage vary with the hydrogen chemical potential (μ_H, which is related to p_{O_2}) and the basal plane termination (T_x^b). Due to this variation in transition points established in the previous section, the region between −1.2 and −1.0 eV represents a complex regime where multiple combinations of basal and edge terminations may coexist and where the overall system stability is strongly edge dependent. For instance, when the basal plane is terminated by oxygen (T_x^b = O), the most stable edge in this range is the {010} Ti edge with 2 monolayers (MLs) of O. In contrast, when the basal plane is terminated by fluorine (T_x^b = F), the most stable edge is the {110} edge with a 1 ML O termination.

Given this complexity, we use the transition point for the {010} C nanoribbon (μ_H = −1.0 eV)—the highest μ_H value among the three nanoribbons—as the reference limit for comparing terminations. This choice is justified because it represents the most reducing condition under which a change in the favored T_x^b is observed across at least one nanoribbon type. While this approximation does not capture the full complexity of intermediate μ_H ranges, it allows us to systematically explore edge stability for well-defined T_x^b values. In the F-terminated basal plane regime (μ_H > −1.0 eV), Fig. 4 shows that the most stable edge configuration varies with varying μ_H values. Between 0 and −0.41 eV, the {110} edge with 1 ML of hydrogen is favored. As the μ_H value decreases from −0.6 to −0.83 eV, a 1 ML F termination becomes more favorable. Below −0.83 eV, the most stable edge switches to the {010} Ti edge terminated with 2 MLs of oxygen.

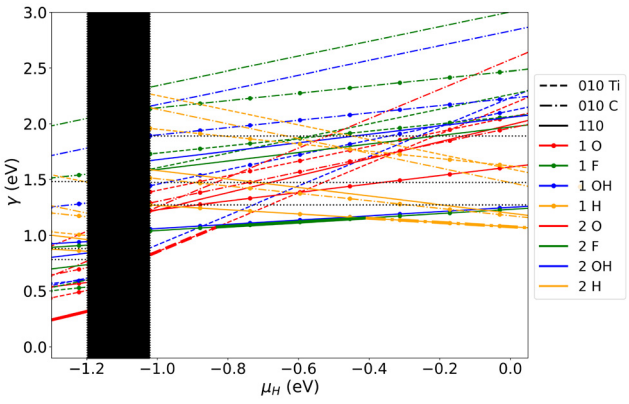

Fig. 4 Stability diagram of $Ti_2CT_x^b$ NRs with edge termination T_x^e being either O, OH, F, or H with different coverages combined with T_x^b = F for which F-termination is stable in the −1 eV < μ_H < 0 eV range and T_x^b = O for which O-termination is stable for μ_H < −1 eV.

Once the μ_H value decreases below −1.2 eV (oxidizing conditions), Fig. 4 shows that the most stable edge is the {110} edge terminated with 1 ML of O. This again emphasizes how both edge and basal terminations respond dynamically to changes in the chemical environment, with stability trends that are coupled across the nanoribbon geometry.

3.3 Thermodynamics of nanoparticles with different edges

From the edge free energies of the stability diagram, we calculated Wulff constructions at every transition point indicated in the stability diagrams in Fig. 4. The top half of Fig. 5 shows how the NP shape changes from μ_H = 0 eV to μ_H = −1 eV. For this chemical potential region, T_x^b = F as identified above. At μ_H = 0 eV, the 2D-nanoparticle is predicted to be a dodecagon with alternating {010} C and {110} edges terminated with T_x^e = 1 ML of H. The shape of the 2D-nanoparticle remains the same until μ_H = −0.41 eV at which point the 2D-nanoparticle becomes a hexagon exposing the {110} edge terminated by a combination T_x^e = 1 ML of H. At μ_H = −0.83 eV, the NP becomes a dodecagon with alternating {010} Ti and {110} edges functionalized with 2 MLs of O and 1 ML of F, respectively. At μ_H = −1.02 eV, the NP is a hexagon with {110} edges with T_x^2 = 2 ML O.

As seen in Fig. 4, for μ_H values between −1.02 and −1.2 eV, the system likely enters a mixed regime where both T_x^b = F and T_x^b = O basal plane terminations may coexist. This chemical potential range is complex and may involve a combination of terminations across different nanoribbon types. As such, a more detailed computational analysis would be required to fully capture the interplay of edge and basal terminations in this region. However, since T_x^b = O is thermodynamically relevant for μ_H < −1.02 eV, we construct Wulff diagrams at μ_H = −1.02 eV and −1.25 eV using T_x^b = O to explore the equilibrium particle shapes in this oxidizing regime. At μ_H = −1.02 eV, the resulting 2D-nanoparticle is primarily hexagonal, exposing 110 edges terminated with 2 MLs of oxygen, while some 010 Ti edges terminated with fluorine appear at the corners. At μ_H = −1.25 eV, the hexagonal shape persists, and the 110 edges remain dominant with full oxygen termination. Overall, while the edge termination (T_x^e) varies somewhat with the basal plane chemistry, the most significant impact of T_x^b is on the type of edge exposed—*i.e.*, which crystallographic edge becomes most thermodynamically favorable—rather than the precise nature of the terminating group.

We note that while the Wulff constructions presented here provide insight into the thermodynamically favorable shapes of MXene 2D-nanoparticles, these specific shapes have not yet been observed experimentally. This is likely due to the fact that MXenes are typically synthesized using top-down etching from MAX phases, where the particle morphology is largely inherited from the parent crystal structure and etching conditions. In contrast, Wulff constructions are most applicable to bottom-up synthesis routes, where particle shapes evolve under thermodynamic control. Nevertheless, these equilibrium shapes offer valuable insight into edge energetics and could help guide future synthetic efforts aimed at controlling

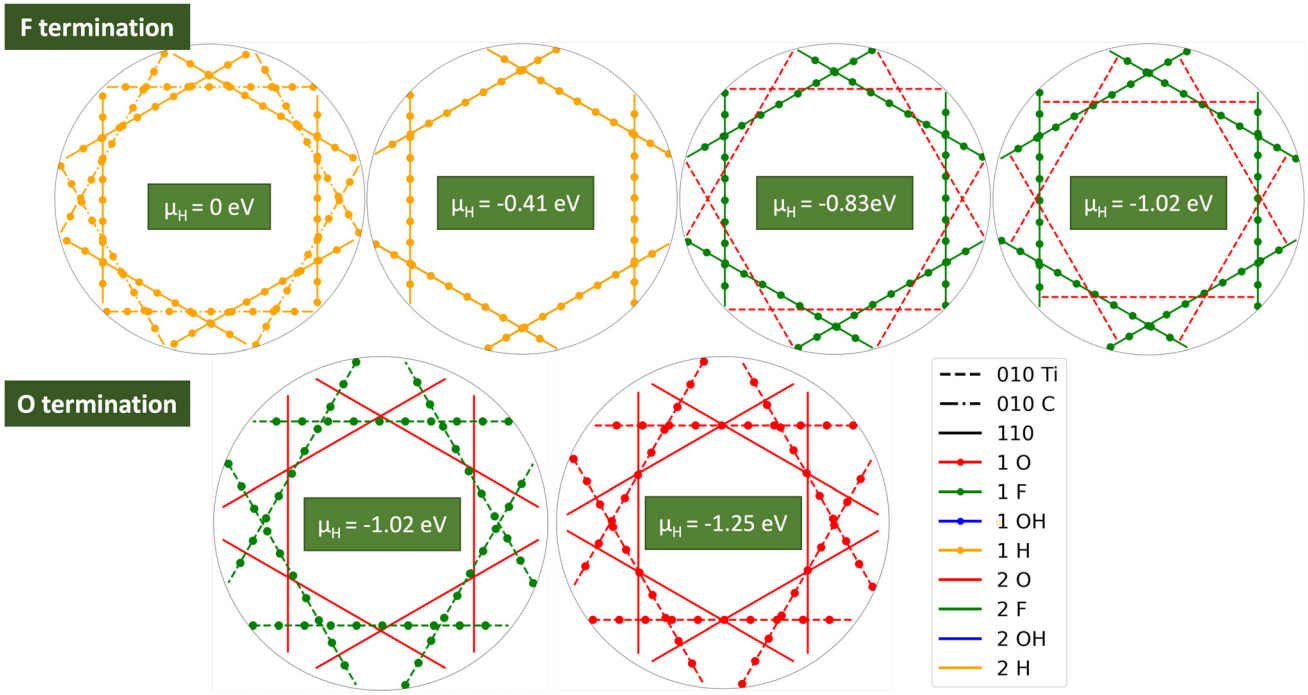

Fig. 5 Wulff constructions of Ti_2CT_x at different chemical potentials where the dominating termination changes from F to O at μ_H = −1 eV. These results are based on the results from the basal plane and edge termination stability analysis.

edge exposure or developing bottom-up methods for the synthesis of MXene nanoparticles. From Fig. 4 and 5, we draw the conclusion that there exists a transition region at around −1 eV where the terminating groups on the 2D-nanoparticle basal planes are a combination of T_x^b = O and F. The Wulff constructions for both of these T_x^b each considered individually predict the 2D-nanoparticle to be hexagonal with different exposed edges that are terminated with different functional groups T_x^e. This leads us to conclude that the 2D-nanoparticle in that region would be a dodecagon with {110} and {010} Ti edges terminated by T_x^e = O assuming that the effects of the terminations T_x^b = O and F are equivalent.

3.4 Probing the MXene edges for hydrogen adsorption chemistry

Fig. 6 shows how hydrogen adsorption energies of single adsorbed H atoms vary across different nanoribbon edges ({010} Ti, {010} C, and {110}) and T_x^e configurations (1 ML F, 2 ML F, 1 ML 0H, 2 ML 0H, 1 ML 0, and 2 ML 0). The color gradient represents the adsorption energy strength, with blue corresponding to more favorable (lower) adsorption energies and red corresponding to less favorable (higher) values. Among the nanoribbon edges, the {010} C edge consistently shows the most favorable hydrogen adsorption, with strongly negative values, *e.g.* −0.77 eV for 1 ML F, −1.14 eV for 2 ML F and −1.88 eV for 2 ML 0H, for all T_x^e configurations. In contrast, Ti edges generally exhibit higher and less favorable adsorption energies, reaching values as high as 2.74 eV for 2 ML F and 2.64 eV for 1 ML 0H, particularly in configurations 1

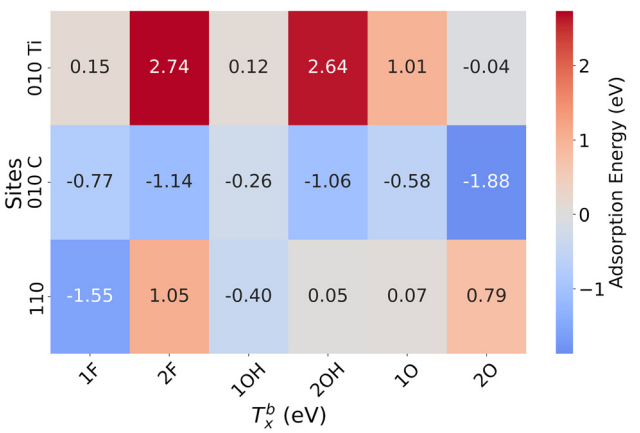

Fig. 6 Most stable adsorption energies of single hydrogen adsorbed on the {010} C, {010} Ti, and {110} edge sites of Ti_2CO_2, *i.e.*, (T_x^b = O), with different edge terminations T_x^e = 1 ML F, 2 ML F, 1 ML OH, 2 ML OH, 1 ML 0, or 2 ML 0.

ML F and 2F. Mixed edges display a range of adsorption energies, including moderately unfavorable values like 1.05 eV for 2F and favorable values such as −1.55 eV for 1 ML F, suggesting more tunable hydrogen chemistry behavior. As T_x^e progresses from 1/2 ML F to 1/2 ML O, the hydrogen adsorption energies for the {010} Ti edges decrease, with values reducing from 2.74 eV in 2 ML F to 1.01 eV in 1 ML O and 0.07 eV in 2 ML O, indicating improved adsorption. Meanwhile, the C edges remain consistently favorable across all configurations.

These trends highlight the {010} C edges as the most suitable for hydrogen adsorption, while changes in T_x^e significantly influence the adsorption behavior of the Ti and mixed edges, with 1 ML O and 2 ML O terminations showing more favorable hydrogen adsorption properties compared to the other terminations and coverage pairs. In cases where the adsorption energy is particularly favorable, it is likely that additional hydrogen atoms could adsorb at those edges; this is further explored in the next section and in the ESI.† This suggests that material and structural modifications could be used to tune the hydrogen adsorption and potentially optimize it for different applications.

3.5 Evaluating hydrogen evolution reaction (HER) potential on MXene edges

For each considered edge, we calculated the computational HER overpotential at 300 K and compared it to the known overpotential for the Ti_2CO_2 2D sheet basal plane (−0.308 V (ref. 20)). We found that the best edge and the edge termination with the lowest computational overpotential for the HER is the {010} C edge terminated with T_x^e = 1 ML OH and T_x^b = O (see Fig. 7 and 8). Importantly, however, based on the stability plots and Wulff constructions, we know that these edge terminations are not thermodynamically stable for any of the conditions considered (oxidizing/reducing). Combining the knowledge from the stability diagrams with what we understand from the volcano plot, we can conclude that under oxidizing conditions, the best HER overpotential at an edge would be −0.08 V for the {010} Ti edge terminated with T_x^e = 1 ML O (see Fig. 7).

For Ti_2CF_2, we find that the {010} Ti edge terminated with T_x^e = 2 MLs of O has the lowest HER overpotential at −0.01 V (see Fig. 8). However, this occurs under very reducing conditions; furthermore, this combination of T_x^e = 2 ML O and T_x^b = F is impossible. In the realm of what is possible, the lowest HER overpotential is found for the {010} C edge terminated with T_x^e = 2 ML F at 0.34 V which is close to the previously calculated basal plane overpotential for Ti_2CO_2 (−0.308 V).[20]

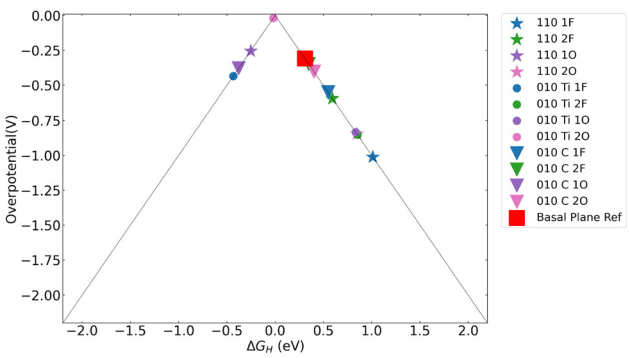

Fig. 7 HER volcano plot with computational overpotentials of Ti_2CO_2 for the 3 types of edges considered and their various terminations: T_x^e = O, OH, and F at 1 and 2 ML coverages.

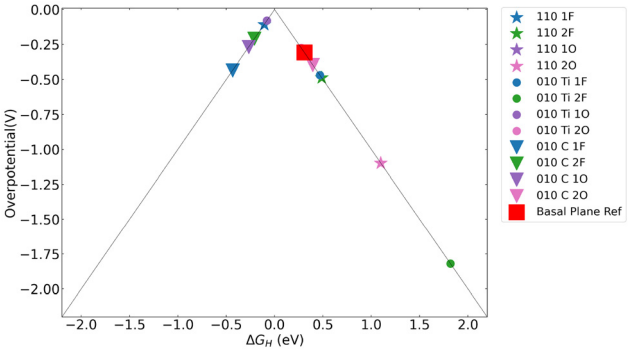

Fig. 8 HER volcano plot with computational overpotentials of Ti_2CF_2 for the 3 types of edges considered and their various terminations: T_x^e = O, OH, and F at 1 and 2 ML coverages.

4 Conclusions

This study provides a comprehensive computational investigation into the structural and chemical characteristics of edges present in a Ti_2C MXene, emphasizing their role and importance in material properties. By systematically exploring the edges in both nanoribbon and 2D-nanoparticle models, we demonstrate that MXene edges exhibit unique properties that differ significantly from the basal planes, driven by undercoordination and symmetry variations. Our findings highlight that edge terminations and functionalizations are dictated by both the basal plane chemistry and the environmental chemical potential, revealing an intricate interplay between structure, chemistry, and stability.

Under reducing conditions, the basal planes favor F-termination, whereas oxidizing conditions lead to O-termination. These trends extend to the edges, where different terminations and coverage emerge depending on the environmental conditions. The edge stability diagrams and Wulff constructions predict that Ti_2CT_x 2D-nanoparticles adopt various shapes, transitioning between hexagonal and dodecagonal morphologies as a function of the chemical potential of hydrogen with different basal plane and edge functional group pairs T_x^b and T_x^e. This underscores the tunability of MXene 2D-nanoparticles for specific applications, with shape and exposed edge terminations optimized for given environmental conditions.

Furthermore, our analysis of hydrogen adsorption chemistry and computational HER overpotentials identifies specific edge terminations, such as {110} and {010} edges with appropriate functionalization, which rival or even exceed the catalytic performance previously found in the basal planes of Mo_2C MXenes.[20] Although some configurations demonstrate excellent catalytic potential, they remain thermodynamically unfavorable, suggesting the need for further experimental and theoretical exploration to stabilize these highly active but unstable sites. This study establishes a framework for understanding and leveraging MXene edge chemistry, laying the groundwork for designing MXene-based materials with

enhanced catalytic and functional properties. The findings open avenues for further exploration into under-coordinated sites, enabling the discovery of novel chemistries and applications across diverse fields.

Conflicts of interest

There are no conflicts of interest to declare.

Data availability

The data supporting this article have been included as part of the ESI.†

Acknowledgements

Y. M. would like to thank the Vagelos Institute for Energy Science and Technology (University of Pennsylvania) for support through a graduate fellowship. A. V. acknowledges the Canadian Institute for Advanced Research (CIFAR) for support through the Accelerated Decarbonization Program. Y. M. and A. V. acknowledge the use of the resources of the National Energy Research Scientific Computing Center, a DOE Office of Science User Facility supported by the Office of Science of the U.S. Department of Energy under contract no. DE-AC02-05CH11231 using the NERSC award BES-ERCAP0023161. We acknowledge funding from U.S. National Science Foundation under Grant Number CHE-2318105 (M-STAR CCI).

References

1 M. Naguib, O. Mashtalir, J. Carle, V. Presser, J. Lu, L. Hultman, Y. Gogotsi and M. W. Barsoum, *ACS Nano*, 2012, **6**, 1322–1331.
2 M. Naguib, M. Kurtoglu, V. Presser, J. Lu, J. Niu, M. Heon, L. Hultman, Y. Gogotsi and M. W. Barsoum, *Adv. Mater.*, 2011, **23**, 4248–4253.
3 M. Naguib, V. N. Mochalin, M. W. Barsoum and Y. Gogotsi, *Adv. Mater.*, 2014, **26**, 992–1005.
4 J. Björk and J. Rosen, *Chem. Mater.*, 2021, **33**, 9108–9118.
5 L. Hong, R. F. Klie and S. Öğüt, *Phys. Rev. B*, 2016, **93**, 115412.
6 B. Jiang, T. Yang, T. Wang, C. Chen, M. Yang, X. Yang, J. Zhang and Z. Kou, *Chem. Eng. J.*, 2022, **442**, 136119.
7 X. Yang, N. Gao, S. Zhou and J. Zhao, *Phys. Chem. Chem. Phys.*, 2018, **20**, 19390–19397.
8 K. Maleski, C. E. Ren, M.-Q. Zhao, B. Anasori and Y. Gogotsi, *ACS Appl. Mater. Interfaces*, 2018, **10**, 24491–24498.
9 M. V. Bollinger, K. W. Jacobsen and J. K. Nørskov, *Phys. Rev. B: Condens. Matter Mater. Phys.*, 2003, **67**, 085410.
10 M. V. Bollinger, J. V. Lauritsen, K. W. Jacobsen, J. K. Nørskov, S. Helveg and F. Besenbacher, *Phys. Rev. Lett.*, 2001, **87**, 196803.
11 H. Schweiger, P. Raybaud, G. Kresse and H. Toulhoat, *J. Catal.*, 2002, **207**, 76–87.
12 D. Cao, T. Shen, P. Liang, X. Chen and H. Shu, *J. Phys. Chem. C*, 2015, **119**, 4294–4301.
13 B. Hinnemann, P. G. Moses, J. Bonde, K. P. Jørgensen, J. H. Nielsen, S. Horch, I. Chorkendorff and J. K. Nørskov, *J. Am. Chem. Soc.*, 2005, **127**, 5308–5309.
14 J. Bonde, P. G. Moses, T. F. Jaramillo, J. K. Nørskov and I. Chorkendorff, *Faraday Discuss.*, 2009, **140**, 219–231.
15 J.-F. Paul and E. Payen, *J. Phys. Chem. B*, 2003, **107**, 4057–4064.
16 M. C. Zonnevylle, R. Hoffmann and S. Harris, *Surf. Sci.*, 1988, **199**, 320–360.
17 C. K. Gan and D. J. Srolovitz, *Phys. Rev. B: Condens. Matter Mater. Phys.*, 2010, **81**, 125445.
18 W. Lee, D. Hedman, J. Dong, L. Zhang, Z. Lee, S. Y. Kim and F. Ding, *Phys. Rev. B*, 2023, **107**, 245420.
19 Z. Zhang, Y. Liu, Y. Yang and B. I. Yakobson, *Nano Lett.*, 2016, **16**, 1398–1403.
20 Z. W. Seh, K. D. Fredrickson, B. Anasori, J. Kibsgaard, A. L. Strickler, M. R. Lukatskaya, Y. Gogotsi, T. F. Jaramillo and A. Vojvodic, *ACS Energy Lett.*, 2016, **1**, 589–594.
21 M.-F. Lin and F.-L. Shyu, *J. Phys. Soc. Jpn.*, 2000, **69**, 3529–3532.
22 Y. Liu, A. Dobrinsky and B. I. Yakobson, *Phys. Rev. Lett.*, 2010, **105**, 235502.
23 S. Okada, *Phys. Rev. B: Condens. Matter Mater. Phys.*, 2008, **77**, 041408.
24 M. Ashton, K. Mathew, R. G. Hennig and S. B. Sinnott, *J. Phys. Chem. C*, 2016, **120**, 3550–3556.
25 C. Zhou, D. Wang, F. Lagunas, B. Atterberry, M. Lei, H. Hu, Z. Zhou, A. S. Filatov, D. Jiang, A. J. Rossini, R. F. Klie and D. V. Talapin, *Nat. Chem.*, 2023, **15**, 1722–1729.
26 G. Wulff, *Z. Krystallogr. Mineral.*, 1901, **34**, 449–530.
27 J. K. Nørskov, T. Bligaard, A. Logadottir, J. R. Kitchin, J. G. Chen, S. Pandelov and U. Stimming, *J. Electrochem. Soc.*, 2005, **152**, J23.
28 E. Skúlason, V. Tripkovic, M. E. Björketun, S. Gudmundsdottir, G. Karlberg, J. Rossmeisl, T. Bligaard, H. Jonsson and J. K. Nørskov, *J. Phys. Chem. C*, 2010, **114**, 18182–18197.
29 P. Giannozzi, S. Baroni, N. Bonini, M. Calandra, R. Car, C. Cavazzoni, D. Ceresoli, G. L. Chiarotti, M. Cococcioni, I. Dabo, A. D. Corso, S. de Gironcoli, S. Fabris, G. Fratesi, R. Gebauer, U. Gerstmann, C. Gougoussis, A. Kokalj, M. Lazzeri, L. Martin-Samos, N. Marzari, F. Mauri, R. Mazzarello, S. Paolini, A. Pasquarello, L. Paulatto, C. Sbraccia, S. Scandolo, G. Sclauzero, A. P. Seitsonen, A. Smogunov, P. Umari and R. M. Wentzcovitch, *J. Phys.: Condens. Matter*, 2009, **21**, 395502.
30 P. Giannozzi, O. Andreussi, T. Brumme, O. Bunau, M. B. Nardelli, M. Calandra, R. Car, C. Cavazzoni, D. Ceresoli, M. Cococcioni, N. Colonna, I. Carnimeo,

A. D. Corso, S. de Gironcoli, P. Delugas, R. A. DiStasio, A. Ferretti, A. Floris, G. Fratesi, G. Fugallo, R. Gebauer, U. Gerstmann, F. Giustino, T. Gorni, J. Jia, M. Kawamura, H.-Y. Ko, A. Kokalj, E. Küçükbenli, M. Lazzeri, M. Marsili, N. Marzari, F. Mauri, N. L. Nguyen, H.-V. Nguyen, A. O. de-la Roza, L. Paulatto, S. Poncé, D. Rocca, R. Sabatini, B. Santra, M. Schlipf, A. P. Seitsonen, A. Smogunov, I. Timrov, T. Thonhauser, P. Umari, N. Vast, X. Wu and S. Baroni, *J. Phys.: Condens. Matter*, 2017, **29**, 465901.

31 J. Wellendorff, K. T. Lundgaard, A. Møgelhøj, V. Petzold, D. D. Landis, J. K. Nørskov, T. Bligaard and K. W. Jacobsen, *Phys. Rev. B: Condens. Matter Mater. Phys.*, 2012, **85**, 235149.

32 J. Demaison and A. G. Császár, *J. Mol. Struct.*, 2012, **1023**, 7–14.